Title

Lithium calix[4]arenes: structural studies and use in the ring opening polymerization of cyclic esters

Journal

RSC Advances, 11(19)

ISSN

2046-2069

Authors

Santoro, Orlando

Elsegood, Mark RJ

Teat, Simon J

et al.

Publication Date

2021-03-17

DOI

10.1039/d1ra00175b

Peer reviewed

Lithium calix[4]arenes: structural studies and use in the ring opening polymerization of cyclic esters.

Orlando Santoro,[a] Mark R. J. Elsegood,[b] Simon J. Teat,[c] Takehiko Yamato[d] and Carl Redshaw[a*]

We have structurally characterized a number of lithiated calix[4]arenes, where the bridge in the calix[4]arene is thia (–S–, $L^{S}H_4$), sulfinyl (–SO–, $L^{SO}H_4$), sulfonyl (–SO_2–, $L^{SO2}H_4$), dimethyleneoxa (–CH_2OCH_2–, $L^{COC}H_4$) or methylene (–CH_2–, LH_4). In the case of $L^{4S}H_4$, interaction with LiO*t*Bu led to the isolation of the complex complex $[Li_8(L^{4S})_2(THF)_4]\cdot 5THF$ (**1**·5THF), whilst similar interaction of $L^{4SO}H_4$ led to the isolation of $[Li_6(L^{4SO}H)_2(THF)_2]\cdot 5(THF)$ (**2**·5THF). Interestingly, the mixed sulfinyl/sulfonyl complexes $[Li_8(Calix[4]arene(SO)(SO_2)(SO_{1.68})_2)_2(THF)_6]\cdot 8(THF)$ (**3**·8THF) and $[Li_5Na(L^{SO/3SO2}H)_2(THF)_5]\cdot 7.5(THF)$ (**4**·7.5(THF) have also been characterized. Interaction of LiO*t*Bu with $L^{SO2}H_4$ and $L^{COC}H_4$ afforded $[Li_5L^{4SO2}(OH)(THF)_4]\cdot 2THF$ (**5**·2THF) and $[Li_6(L^{COC})_2(HOtBu)_2]\cdot 0.78THF\cdot 1.22hexane$ (**6**·0.78THF·1.22hexane), respectively. In the case of LH_4, reaction with LiO*t*Bu in THF afforded a monoclinic polymorph $[LH_2Li_2(thf)(OH_2)_2]\cdot 3THF$ (**7**·3THF) of a known triclinic form of the complex, whilst reaction of the de-butylated analogue of LH_4, namely de-BuLH_4, afforded a polymeric chain structure $\{[Li_5(de\text{-}BuL)(OH)(NCMe)_3]\cdot 2MeCN\}_n$ (**8**·2MeCN). For comparative catalytic studies, the complex $[Li_6(L^{Pr})_2(H_2O)_2]\cdot hexane$ (**9**·hexane), where $L^{Pr2}H_2$ = 1,3-di-*n*-propyloxycalix[4]areneH_2, was also prepared. The molecular crystal structures of **1** - **9** are reported, and their ability to act as catalysts for the ring opening (co-)/polymerization (ROP) of the cyclic esters ε-caprolactone, δ-valerolactone, and *rac*-lactide has been investigated. In most of the cases, complex **6** outperformed the other systems, allowing for higher conversions and/or greated polymer M_n.

Introduction

The search for alternative plastics to petroleum-based products continues at a pace. One avenue of exploration is to develop new, greener biodegradable polymers, but which retain the desirable features of traditional plastics. [1] With this in mind, one promising route is to exploit the ring opening polymerization (ROP) of cyclic esters, a process which can be controlled by a metal-based catalyst. [2] For the catalyst, it is important that the ancillary ligands present can be easily adjusted in terms of their steric and electronic properties. There has been considerable interest in the use of the phenolic macrocycles called calixarenes in a broad range of catalysis. [3] Indeed, we have been interested in employing such species in the ROP of cyclic esters to afford biodegradable polymers. [4] Both the upper- and lower-rim of a calixarene can readily be modified, and for the latter the introduction of ether groups allows the charge to be altered. [5] Moreover, different bridging groups can be used to link the phenols, and the range of conformations available to calixarenes allows for further structural flexibility. [6] In terms of the metal employed, it is important it is relatively cheap and non-toxic. Lithium is the 25th most abundant element, and lithium systems have shown promise as ROP catalysts. [7] Over the last decade or so, a number of routes to lithiated calix[4]arenes and their thia-bridged analogues have been developed. The early work on calix[*n*]arenes involved the use of ^{7}Li NMR spectroscopy, [8] whilst for p-*tert*-butylcalix[4]areneH_4 (L^4H_4), early structural work involved the use of lithium amide, [9] whilst Davidson *et al* employed *n*BuLi in the presence of either wet or dried hexamethylphosphoramide (hmpa) and isolated $Li_4L^4{\cdot}LiOH{\cdot}4hmpa$ or $[Li_4L^4{\cdot}2hmpa]_2$, respectively. [10] Floriani *et al* also employed *n*BuLi in the presence of naphthalene to prepare lithiated calix[4]arenes. [11] Fromm *et al* structurally characterized the complex $[Li_4(LH_2)_2(THF)_4]\cdot 3THF$, possessing a core containing two face-shared Li_4O_4 cubes from the reaction of L^4H_4 and LiO*t*Bu; the partial hydrolysis product $[Li_2(L^4H_2)(H_2O)(\mu\text{-}H_2O)(THF)]\cdot 3THF$ was also characterized. [12] Hanna *et al* also studied reactions of calix[4 and 8]arene as well as p-*tert*-butylcalix[4 and 8]arene with LiO*t*Bu or $LiOSiMe_3$ respectively, and isolated monoanions. [13] In later studies, Hanna *et al* extended their studies to the reaction of p-*tert*-butylcalix[5]areneH_5 with a number of lithiated reagents, namely LiOH, *n*BuLi and LiH. [14] Moreover, a number of molybdocalix[4]arenes incorporating lithium, primarily as part of a bridging ligand have also been reported, [15] as have mixed lithium-strontium complexes. [16] We have previously structurally characterized the two complexes $[L^4H_2(OMe)(OLi)]_2\cdot 4MeCN$ and $\{L^4H_2(OLi)[OLi(NCMe)_2]\}_2\cdot 8MeCN$ resulting from the use of *n*BuLi. [17]

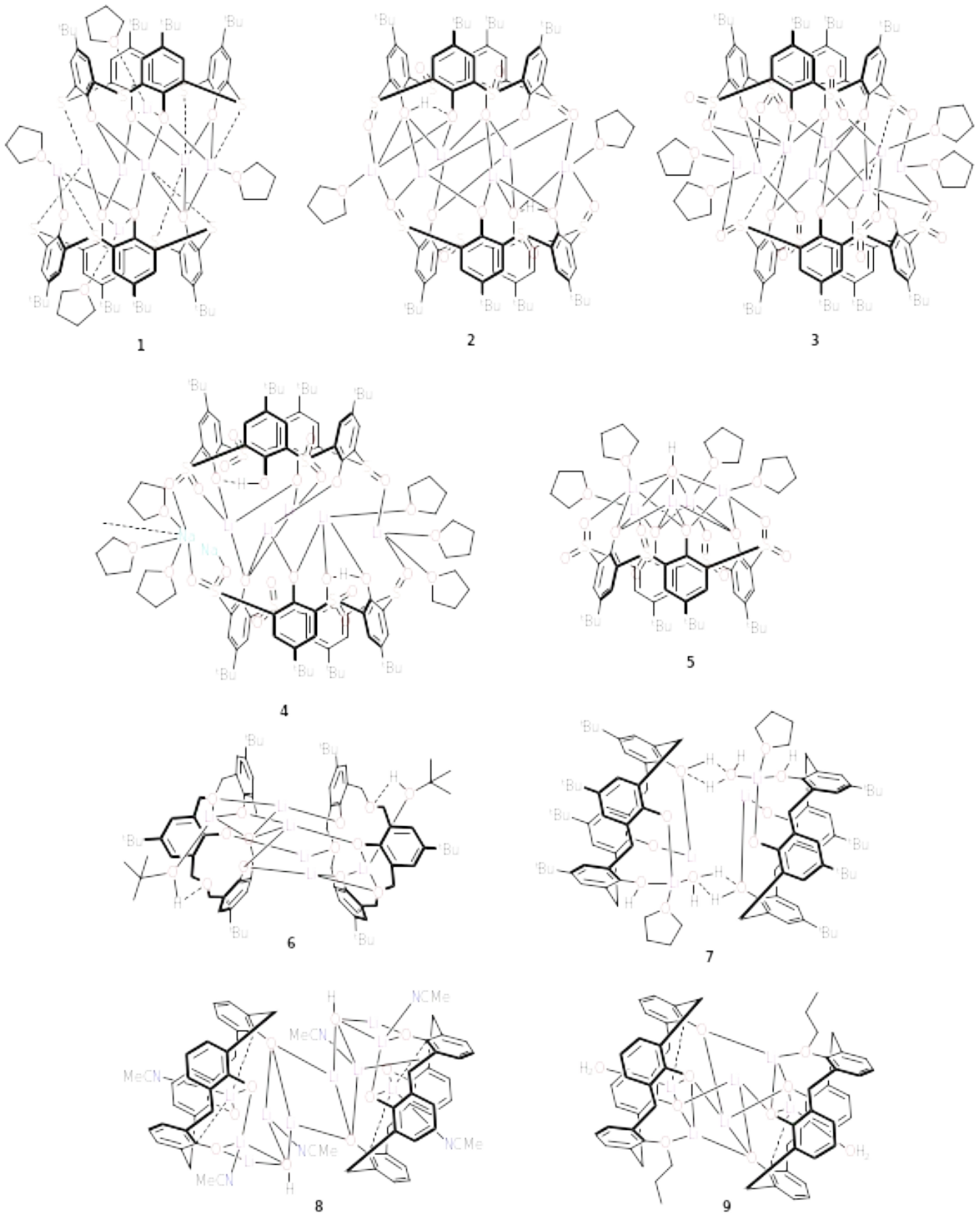

Chart 1. Lithium-calixarene complexes **1** – **9** prepared herein.

For p-*tert*-butyltetrathiacalix[4]areneH_4 ($L^{S4}H_4$), Zeller and Radius employed *n*BuLi to access $L^{S4}Li_4$, which proved problematic to crystallize and only the decomposition product $[L^{S4}Li_5(OH)(THF)_4]$ was structurally characterized; the complex

could be isolated directly using $LiOH{\cdot}H_2O/L^{S4}H_4$. [18] We have reacted a lower rim 1,3-diacid calix[4]arene with either Li_2CO_3 or *t*BuLi and isolated helical nanotubes or infinite chains, respectively. [19] The structure of a supramolecular lithium calix[4]arene complex has also been reported. [20]

Despite this synthetic activity, applications of such lithiated calixarene species have not been forthcoming. With this in mind, we have embarked upon a programme to screen the potential for lithiated calixarenes for the ring opening polymerization (ROP) of cyclic esters. Herein, we present our findings on calix[4]arene systems for which the calixarene bridge has been varied, *viz* –S– ($L^{4S}H_4$), –SO– ($L^{4SO}H_4$), $–SO_2–$ ($L^{4SO2}H_4$), $–CH_2OCH_2–$ ($L^{COC}H_4$), $–CH_2–$ (L^4H_4), and in the case of the latter 1,3-*n*-propoxide groups have also been introduced at the lower-rim. Structural studies and the ROP of the cyclic esters ε-caprolactone, δ-valerolactone and *rac*-lactide are reported. The nine lithium-calixarenes prepared herein are shown in chart 1. We note that a number of lithium-containing cages, rings, and ladders, supported primarily by phenolate-type ligation, have previously been employed for the ROP of cyclic esters. [21] The use of calixarenes though, is somewhat limited. [4, 22]

Results and discussion,

Syntheses and solid-state structures

-thia-

Of the number of synthetic routes to lithiated calixarenes outlined above, [9-14] we chose as our entry point the use of Li*O*t*Bu. Reaction of Li*O*t*Bu (5 equiv.) with $L^{4S}H_4$ led to the isolation of the complex $[Li_8(L^{4S})_2(THF)_4]{\cdot}5THF$ (**1**·5THF). Single crystals were grown, in *ca*. 65% isolated yield, from a saturated THF solution at ambient temperature and an X-ray structure determination revealed the structure shown in Figure 1; for an alternative view of the core see Figure S1, ESI.] Table 5 presents the crystal data for this and the other crystal structures reported herein. A closely related structural motif has been reported previously for $[Li_4L^4.2hmpa]_2$ (see below, chart 2), whilst related sodium and potassium-containing motifs have also been reported. [4, 12, 13]

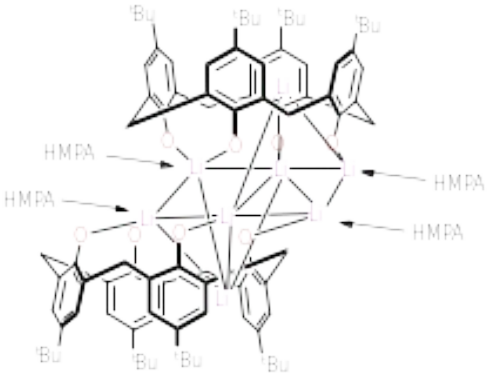

Chart 2. Structure of $[Li_4L^4.2hmpa]_2$. [10]

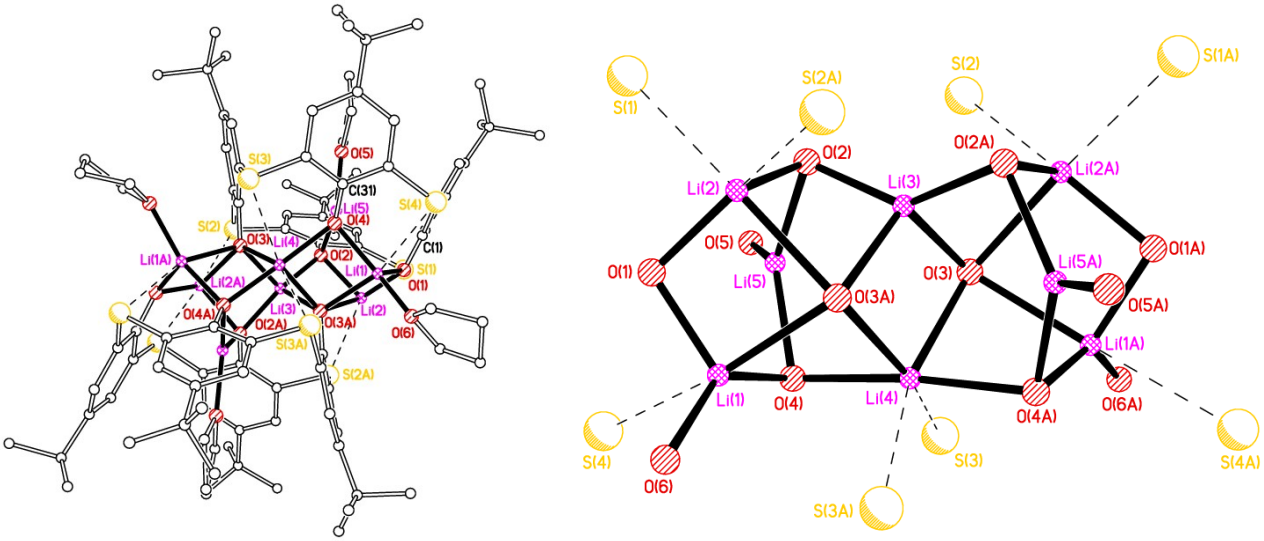

Figure 1. Molecular structure (left) and core (right) of $[Li_8(L^{4S})_2(THF)_4]{\cdot}5THF$ (**1**·5THF). H atoms, minor disorder components and non-coordinated THFs omitted for clarity. Selected bond lengths (Å) and angles (°): Li(1)–O(1) 1.810(16), Li(1)–O(3A) 2.193(16), Li(1)–O(4) 1.947(18), Li(1)–O(6) 1.967(18), Li(3)–O(2) 1.882(8), Li(3)–O(3) 1.966(13), Li(4)–O(4) 2.046(6), Li(5)–O(2) 1.930(16), Li(5)–O(4) 1.951(17), Li(5)–O(5) 1.964(17); Li(1)–O(1)–Li(2) 96.8(8), Li(3)–O(3)–Li(4) 78.8(6), O(4)–Li(4)–O(4A) 174.3(11), O(2)–Li(5)–O(4) 119.9(8).

The molecule lies on a 2-fold axis which passes through Li(3)···Li(4). Thus, half of the molecule is unique as are 2½ THF molecules of crystallization. The ½ THF was modelled using Platon Squeeze. [23] All four S atoms make contacts with one or more lithium centres, namely Li(1)···S(4) = 2.720(15), Li(2)···S(1) = 2.610(17) ,Li(2)···S(2A) = 2.644(15), Li(4)···S(3) = 2.734(10), Li(4)···S(3A) = 2.734(10) Å. Furthermore, Li(5) is involved in C(π) contacts, *viz* Li(5)•••C(1) = 2.74(2) and Li(5)•••C(31) = 2.670(18) Å. In the packing of **1**, the calixarene complexes are well separated with THFs in the voids. The compound is not so soluble in toluene, which is problematic for the ROP studies *vide infra*.

Sulfinyl

Interaction of LiO*t*Bu with $L^{4SO}H_4$ afforded small prisms of $[Li_6(L^{4SO}H)_2(THF)_2]\cdot5(THF)$ (**2**·5THF) in *ca*. 30% yield on standing (2 days) at ambient temperature. The molecular structure was determined using synchrotron radiation, and is shown in figure 2; the core is shown in Figure S2, ESI. Whilst the data was weak, the connectivity was clearly established. The molecule lies on a centre of symmetry, and so half is unique. Given there are six lithium ions present, and analysis of the bond lengths and relative positions of the phenolate oxygens, we conclude that O(3) is protonated; the position of O(2) also suggests it forms an H-bond with O(3). Two of the SO oxygens bind to lithium centres namely Li(1) and Li(3), whilst Li(2) remains 4-coordinate. The phenolate oxygens O(2) and O(3) bridge three lithium centres, whilst O(1) and O(4) bridge only two Li centres. The SO groups have the O partially disordered at the alternative tetrahedral site on the S with minor component occupancies between *ca*. 0.1-0.2.

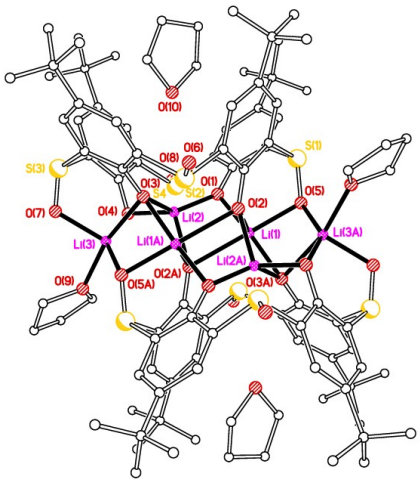

Figure 2. Molecular structure of $[Li_6(L^{4SO}H)_2(THF)_2]\cdot5(THF)$ (**2**·5THF). H atoms and minor disorder components omitted for clarity. Selected bond lengths (Å) and angles (°): Li(1)–O(1) 1.947(12), Li(1)–O(2) 1.973(10), Li(1)–O(2A) 1.956(14), Li(1)–O(3A) 1.940(12), Li(1)–O(5) 2.038(12), Li(2)–O(1) 1.791(17), Li(2)–O(2A) 1.956(14), Li(2)–O(3) 2.037(15), Li(2)–O(4) 1.847(18), Li(3)–O(3) 2.228(12), Li(3)–O(5A) 2.072(12), Li(3)–O(7) 1.936(14), Li(3)–O(9) 1.996(12); O(1)–Li(1)–O(2) 94.9(5), O(1)–Li(2)–O(4) 119.5(8), O(3)–Li(3)–O(7) 96.6(5).

On one occasion, reaction of $L^{4SO}H_4$ with LiO*t*Bu led to the isolation of a mixed sulfinyl/sulfonyl complex, namely $[Li_8(L^{SO/3SO2})_2(THF)_6]\cdot8(THF)$ (**3**·8THF). The molecular structure is shown in Figure 3 (for an alternative view, see Figure S3, ESI), with selected bond lengths and angles given in the caption. The molecule lies on a centre of symmetry, and so half of this formula is unique. Interestingly, only one of the bridging S centers on each calix {S(2)} has just one O group bound (*i.e*. a sulfinyl), whilst the other three have two oxygens (*i.e*. sulfonyls), though it should be noted two of these actually have *ca*. 1.68 oxygens rather than 2, indicating some slight variability in the degree of oxidation at sulfur in these calixarenes. There are weak Li(1)···S(2') and Li(2)···S(2') interactions of 2.928(5) and 3.098(5) Å, respectively, which are both longer than seen in **1**·5THF. Each calixarene possesses a cone conformation. The molecules pack forming layers in the *b*/*c* plane (see Figure S4, ESI). The presence of the sulfonyl [–SO_2–] bridges was thought to arise from adventitious oxidation during the reaction; mass spectra of the parent $L^{4SO}H_4$ did not exhibit higher peaks associated with the presence of -SO_2- bridges.

We also isolated a Na-bridged polymer $[Li_5Na(L^{SO/3SO2}H)_2(THF)_5]\cdot7.5(THF)$ (**4**·7.5(THF) from the reaction of $L^{4SO}H_4$ with LiOH. The molecular structure is shown in Figure 4, with selected bond lengths and angles given in the caption. Both Li(1) and Li(4) are distorted squared-based pyramidal, whilst Li(2) is distorted octahedral and Li(5) distorted tetrahedral. Li(3), whilst forming 4 bonds to neighbouring oxygens, also forms two weaker interactions to S(2) and S(6). For all but one of the SO_2 groups present, one of the oxygen atoms binds to Li or Na, whilst for S(5) one O bridges Li(1) and Li(2) and the other bonds to Na(1). In the case of the SO groups, the S binds weakly to Li(3) and the O binds to either Li(5) or Na(1). The slight variability in oxidation at S is manifested here with O(20) being 78.0(18)% occupied.

Complex **4** forms 1D chains linked via octahedral Na^+ ions (Figure 4, right). We have previously noted the incorporation of Na from drying agents in metallocalixarene chemistry. [24] In **4**, to balance the overall charge, two phenols remain protonated, one on each calix[4]arene.

Sulfonyl

Extension of the LiO*t*Bu methodology to the sulfonyl-(–SO_2–) bridged calix[4]arene system, afforded single crystals suitable for X-ray diffraction from a saturated tetrahydrofuran solution at 0 °C in *ca*. 60% isolated yield. The molecular structure of $[Li_5L^{4SO2}(OH)(THF)_4]\cdot2THF$ (**5**·2THF) is shown in Figure 5, with selected bond lengths and angles given in the caption. The complex contains the Li_5OH motif noted by Davidson *et al*, [10] and Zeller and Radius, [18] and, like the latter, lies on a 4-fold axis and possesses four lithium-bound THF ligands. The difference in **5** is that an oxygen of each of the bridging sulfonyl groups is bound to each of the 'outer' lithium centres. The lithium atom Li(2) is 0.580 Å above the plane formed by the phenolate oxygens, whilst the Li(2)–O(5) bond length is 1.958(13) Å *cf* 2.055(10) Å for the Zeller and Radius structure. [18] Each of the lithium centres is 5-coordinate with the other four adopting what can best be described as trigonal bipyramidal geometries, whilst the inner lithium centre Li(2) adopts a square pyramidal geometry. Both the THFs of crystallization are substantially disordered on the 4-fold axis and were modelled as diffuse regions of electron density by using Platon Squeeze. [23] One THF resides in the calixarene cavity, the other lies above the OH beyond the four coordinated THF molecules.

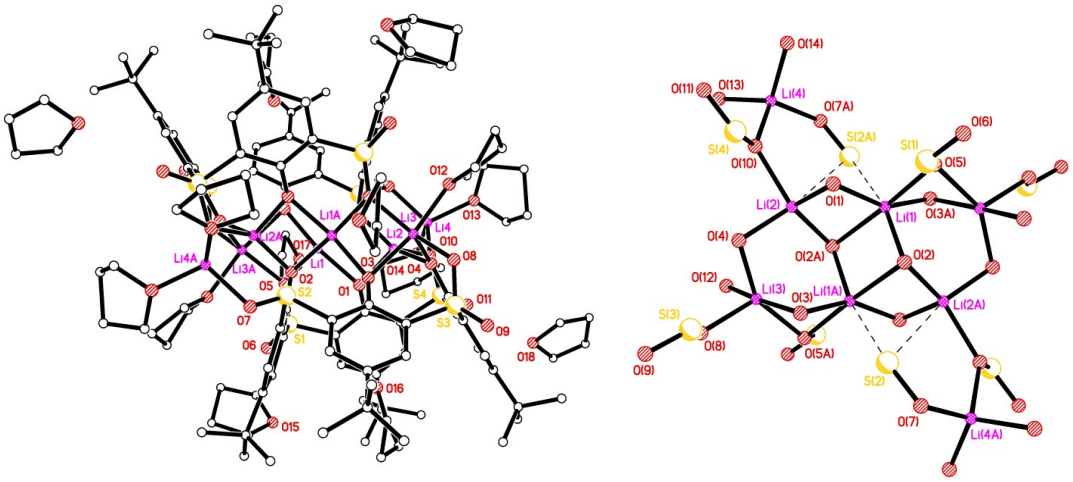

Figure 3. Molecular structure (left) and core (right) of $[Li_8(L^{SO/3SO2})_2(THF)_6]\cdot 8(THF)$ **3**·8(THF). H atoms, and minor disorder components omitted for clarity. Selected bond lengths (Å) and angles (°): Li(1)–O(1) 1.957(5), Li(1)–O(2) 1.954(5), Li(1)–O(2A) 2.247(6), Li(1)–O(5) 2.145(6), Li(2)–O(1) 1.870(6), Li(2)–O(2A) 1.931(6), Li(2)–O(4) 1.852(6), Li(2)–O(10) 2.041(6); Li(1)–O(1)–Li(2) 89.4(2), Li(1)–O(2)–Li(2A) 110.7(2), Li(2)–O(10)–Li(4) 121.8(2).

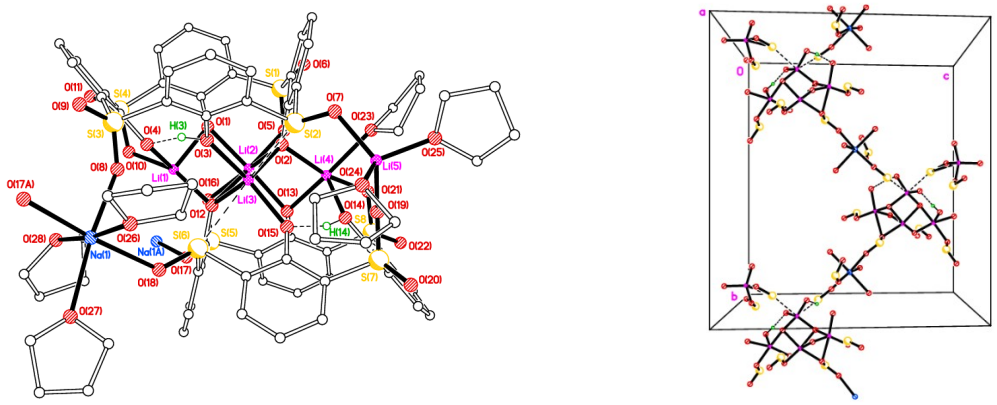

Figure 4. Repeating unit (left) and 1D zig-zag polymer chains (right) in the structure of $[Li_5Na(L^{SO/3SO2}H)_2(THF)_5]\cdot 7.5(THF)$ (**4**·7.5THF). H atoms not involved in H-bonding, minor disorder components and non-coordinated THFs omitted for clarity.Selected bond lengths (Å) and angles (°): Li(1)–O(1) 1.876(8), Li(1)–O(4) 1.970(8), Li(1)–O(10) 1.988(8), Li(1)–O(12) 1.969(8), Li(1)–O(16) 2.352(8), Li(1)–S(4) 2.932(7), Li(2)–O(1) 1.974(8), Li(2)–O(2) 2.081(8), Li(2)–O(5) 2.135(9), Li(2)–O(12) 2.259(8), Li(2)–O(16) 2.147(8), Li(3)–O(2) 1.945(8), Li(3)–O(3) 1.996(7), Li(3)–O(12) 1.926(7), Li(3)–O(15) 2.016(7), Li(3)–S(2) 2.837(7), Li(3)–S(6) 2.968(7); Li(1)–O(1)–Li(2) 83.5(3), Li(1)–O(12)–Li(2) 74.3(3), Li(1)–O(12)–Li(3) 116.8(3), Li(2)–O(2)–Li(3) 87.2(3), Li(2)–O(12)–Li(3) 82.8(3).

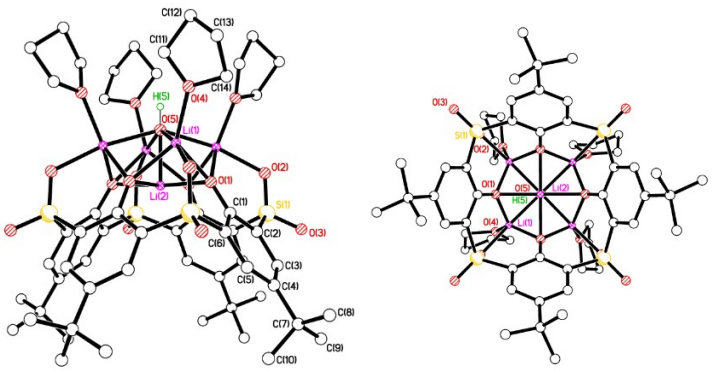

Figure 5. Two perpendicular views of the molecular structure of $[Li_5L^{4SO2}(OH)(THF)_4]\cdot 2THF$ (**5**·2THF). H atoms, minor disorder components and non-cordinated THF omitted for clarity. Selected bond lengths (Å) and angles (°): Li(1)–O(1) 2.002(6), Li(1)–O(4) 1.988(6), Li(1)–O(5) 2.138(6), Li(2)–O(1) 2.018(2), Li(2)–O(5) 1.958(13); Li(1)–O(5)–Li(2) 74.3(2), O(1)–Li(2)–O(5) 87.3(3).

Dimethyleneoxa

Reaction of $L^{COC}H_4$ with Li*O*t*Bu* led, following work-up, to the complex $[Li_6(L^{COC})_2(HO{t}Bu)_2]\cdot 0.78THF\cdot 1.22hexane$ (**6**·0.78THF·1.22hexane) in *ca*. 45% isolated yield. Two views of the molecular structure are shown in Figure 6, with selected bond lengths and angles given in the caption. The core of the complex comprises a pseudo-cubane Li_6O_6 unit, which contains four, boat-shaped, six-membered faces of two Li_3O_3 units. A *t*BuOH molecule is bound to Li(2) and resides within the calixarene cavity and, being disordered, H-bonds to either O(2) (for the major component) or O(6) (minor). Pairs of molecules sit in a slipped face-to-face or cavity-to-cavity motif with *t*BuOH molecules pointing approximately towards each other.

Methylene

In the case of LH_4, reaction with Li*O*t*Bu* (2.2 equiv.) in THF afforded $[LH_2Li_2(THF)(OH_2)_2]\cdot 3THF$ (**7**·3THF), which is a monoclinic polymorph of a known, triclinic, structure reported by Fromm *et al*. [12] The crystals were very small and very weakly diffracting, even at the synchrotron, which resulted in the poor *R* factor. The absolute structure could not be determined due to the combination of radiation wavelength and lack of an anomalous scatterer. The H atoms on the terminal water molecule could not be located in difference maps, but the proximity of this water molecule and two H-bond acceptors is perfectly logical. The H atoms on the bridging waters were placed geometrically, while those between calixarene oxygens are heavily restrained. In reality they are probably more asymmetric. Their presence is required for charge balance and supported by the better, known structure. There are two molecules of the Li_2 complex and six THFs of crystallisation in the asymmetric unit. They form an H-bonded cluster involving both complexes and four THFs (see Figure 7; a view of a single molecule of **7**·3THF is shown in Figure S5, ESI), with an additional THF in each calixarene cavity. The same motif is seen in the published structure. Although the authors suggest that their structure does not have a THF in the cavity, closer inspection reveals it actually has. Also, for each complex, two THFs H-bond to water hydrogens.

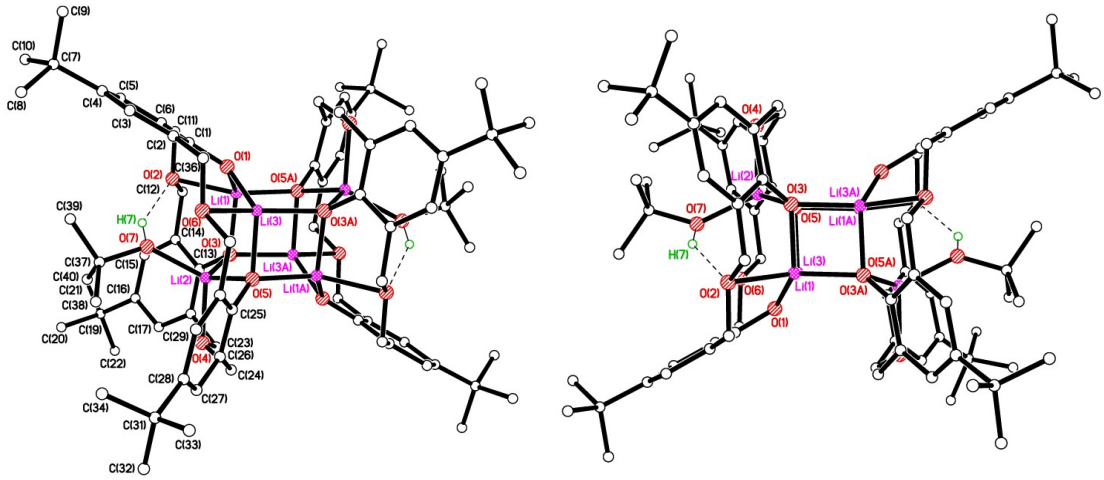

Figure 6. Two views of the molecular structure of $[Li_6(L^{COC})_2(HO{t}Bu)_2]\cdot THF\cdot hexane$ (**6**·THF·hexane). H atoms not involved in H-bonding, minor disorder components and non-coordinated solvent of crystallisation omitted for clarity Selected bond lengths (Å) and angles (°): Li(1)–O(1) 1.861(3), Li(1)–O(2) 2.075(3), Li(1)–O(3) 1.922(3), Li(2)–O(3) 1.940(3), Li(2)–O(5) 1.937(4), Li(2)–O(7) 1.931(4), Li(3)–O(1) 1.859(3), Li(3)–O(3A) 1.915(3); O(1)–Li(1)–O(2) 94.87(13), O(1)–Li(1)–O(3) 127.32(17), O(3)–Li(2)–O(5) 112.94(15).

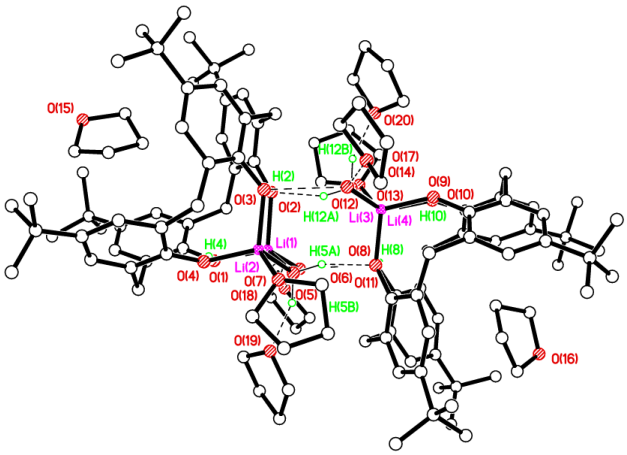

Figure 7. Molecular structure of the H-bonded dimer of $[LH_2Li_2(THF)(OH_2)_2]\cdot 3THF$ (**7**·3THF). H atoms not involved in H-bonding and minor disorder components omitted for clarity Selected bond lengths (Å) and angles (°): Li(1)–O(1) 1.86(3), Li(1)–O(2) 1.99(3), Li(1)–O(5) 1.97(3), Li(1)–O(6) 1.94(3), Li(1)•••Li(2) 3.06(4), Li(2)–O(3) 1.95(3), Li(2)–O(4) 1.89(3), Li(2)–O(5) 2.00(3), Li(2)–O(7) 1.92(3), Li(3)•••Li(4) 3.10(4), Li(1)–O(5)–Li(2) 100.7(12), O(1)–Li(1)–O(2) 104.2(14), O(3)–Li(2)–O(4) 105.3(14).

Similar reaction of the de-butylated analogue of LH_4, namely de-BuLH_4, afforded, following work-up (MeCN), the polymeric chain structure $\{[Li_5(de\text{-}BuL)(OH)(NCMe)_3]\cdot 2MeCN\}_n$ (**8**·2MeCN), and half of this is the asymmetric unit. The molecular structure is shown in Figure 8 (left), with selected bond lengths and angles given in the caption. The structure is a 1D zig-zag chain polymer and a mirror plane bisects the calixarene. The structure was non-merohedrally twinned via a 180° rotation about real axis 0 0 1 with twin components 52.2:47.8(4) %. Four lithium ions at the lower rim of the calixarene are each bridging a pair of oxygens. One lithium ion is in the cavity of the calixarene, bound to two oxygens and π-bonded to two *ipso* carbons and, as a result, a pinched-cone

conformation for the calixarene is observed. The calixarenes are linked via centro-symmetric Li_2O_2 diamonds involving Li(2) and O(2). The Li(3)···C(6) distance is 2.734(6) Å. Li(1), which is not involved in the chain propagation, bears an NCMe ligand, as does Li(3) in the cavity. The complex packs with the 1D zig-zag chain polymer propagating in the *b* direction (Figure 6, right).

For our catalytic studies, we were also interested in evaluating the affect of the presence of alkyl chains at the lower rim. With this in mind, 1,3-di-*n*-propyloxycalix[4]arene, 1,3-$L(OH)_2(nPrO)_2$, which we abbreviate as $L^{Pr2}H_2$, was treated with *n*BuLi in hexane. Following work-up, small crystals suitable for X-ray diffraction using synchrotron radiation were obtained. The molecular structure (Figure 9) revealed the complex to be $[Li_6(L^{Pr})_2(H_2O)_2]$·hexane (**9**·hexane). Half of the complex and half a solvent molecule are unique, both on *i*. The core comprises two face-sharing distorted cubes. The distortion arises because Li(1) and O(3) are not directly bound, and instead Li(1) makes a π-interaction with C(23), which is bound to O(3). Additionally, Li(3) binds to the water molecule which resides in the calixarene cavity. Each calixarene adopts a pinched conformation with rings attached to O(2) and O(4) splayed out, whilst those at O(1) and O(4) are pinched together.

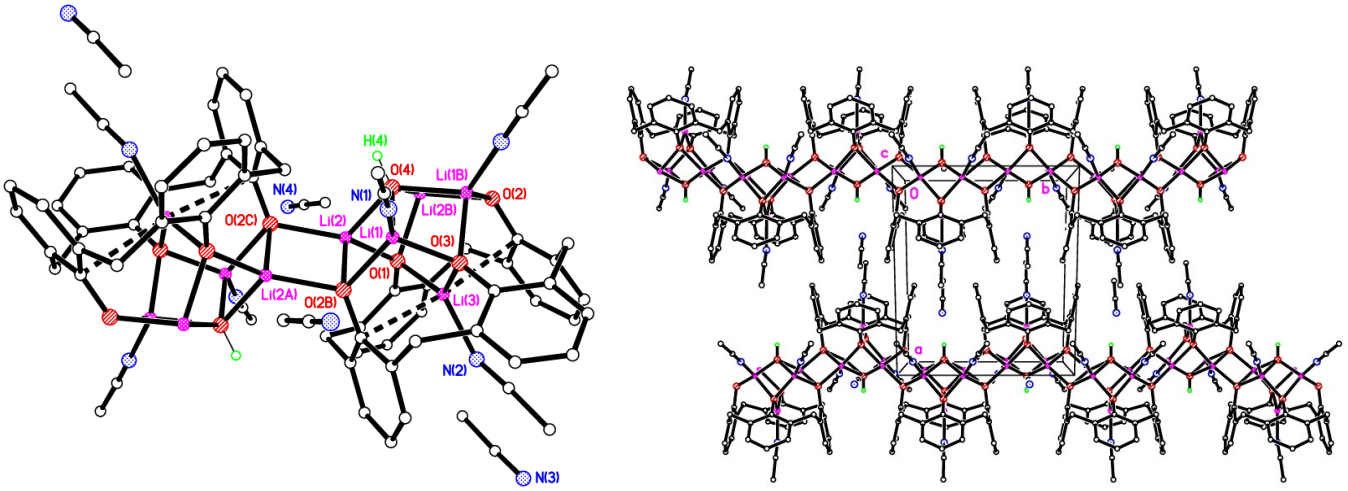

Figure 8. (Left) Molecular structure of the repeating unit in the polymeric structure $\{[Li_5(de\text{-}BuL)(OH)(NCMe)_3]\cdot 2MeCN\}_n$ (**8**·2MeCN); (right) 1D zig-zag chain polymer propagating in the *b* direction. Most H atoms and minor disorder components omitted for clarity. Selected bond lengths (Å) and angles (°): Li(1)–O(2B) 1.999(15), Li(1)–O(3) 1.910(16), Li(1)–O(4) 1.988(14), Li(1)–N(1) 2.071(16), Li(2)–O(1) 1.961(14), Li(2)–O(2B) 1.991(16), Li(2)–O(2) 2.058(13), Li(2)–O(4) 1.944(14); O(2B)–Li(1)–O(3) 104.3(7), O(1)–Li(2)–O(2C) 138.7(7), Li(1B)–O(4)–Li(2) 130.3(6).

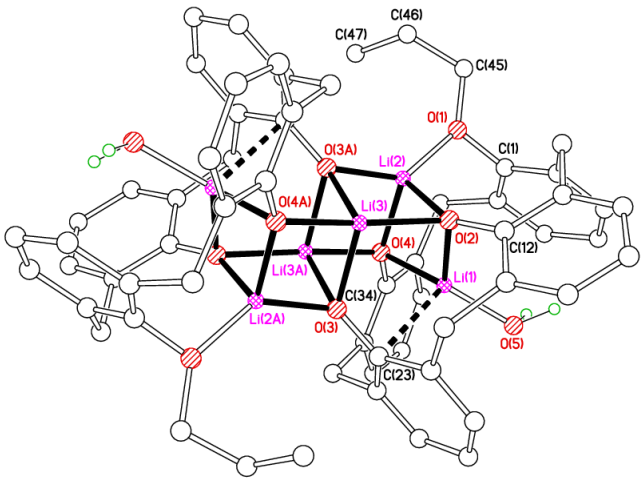

Figure 9. Molecular structure of $[Li_6(L^{Pr})_2(H_2O)_2]$·hexane (**9**·hexane). Most H atoms and hexane of crystallization omitted for clarity. Selected bond lengths (Å) and angles (°): Li(1)–O(2) 1.913(3), Li(1)–O(4) 1.935(3), Li(1)–O(5) 1.885(3), Li(2)–O(1) 1.883(3), Li(2)–O(2) 1.963(3), Li(3)–O(3A) 1.948(3), Li(2)–O(4) 1.973(3); Li(1)–O(2)–Li(2) 78.64(13), Li(1)–O(4)–Li(3A) 102.41(13), O(2)–Li(3)–O(4A) 166.43(16).

ROP Studies

ε-caprolactone (ε-CL)

We have examined the ability of the complexes prepared herein (not **3**) to act as catalysts for the ROP of ε-CL (Table 1). When conducting the reaction in toluene at 130 °C, poor activity was observed upon using a monomer to catalyst ratio of 100:1 and in the presence of one equiv./Li of BnOH as co-activator. In fact, the conversions observed were in the range of 10-20%. The reaction was then repeated under *solvent-free* conditions in the absence of a co-activator (Table 2). While no reactivity was obtained after 24 h for compound **1** and in the presence of the Na-containing species **4** (runs 1 and 4), complete monomer conversion was achieved within 10 minutes in the presence of the dimethyleneoxa-derivative **6** (run 7). Moreover, interesting reactivity was exhibited by the SO_2-bridged congener **5** and the methylene-bridged compound **7**. Indeed, the formation of polymer blocking the stirring of the mixture took place within 1 h, affording 40 and 80% conversion for **5** and **7**, respectively. Good activity was also shown by **2** and **9** (45 and 77% conversion, respectively), albeit requiring longer reaction times. The activity trend (**6** > **7** >**8** > **5** > **9** > **2**) indicated a positive effect of the dimethyleneoxa bridge systems, compared with its $–CH_2–$ and S-containing congeners. Interestingly, similar behaviour has been previously observed

for ethylene polymerization promoted by V-based catalysts. [25] Such higher activity could be attributed to the greater flexibility of the dimethyleneoxa bridge (over $–CH_2–$ and –S–) allowing the monomer better access to active centres and/or to presence of oxygen atoms which help stabilize the active species. With respect to the CH_2-bridged complexes, the higher activity of complex **7** over its de-butylated analogue **8** could be attributed to its higher solubility in the reaction medium. Finally, the lower activity of **9** could be due to the steric encumbrance of its propoxy groups. In all cases, M_n higher than the calculated values were observed, suggesting a concentration of the active species lower than expected. Moreover, the rather broad M_w/M_n values indicated poor control over the polymerization, possibly due to the forcing reaction conditions as well as to the heterogenization of the reaction medium. These factors impeded the rigorous study of the kinetics aspects of the reaction. The ^{1}H NMR spectrum of the PCL synthesized with **6** showed the presence of a triplet at δ 3.6 ppm, compatible with linear $–CH_2OR$ (R = H or *t*Bu) terminated polymers (Figure S6, ESI). This was confirmed by mass spectrometry. In fact, the MALDI-ToF spectrum of the sample (Figure S7) displayed one population of peaks (separated by 114 m/z units) compatible with an α-*t*BuO-ω-OH terminated linear PCL. This suggested that the *tert*-butoxy group of **6** serves as initiating group of the ROP process. Upon performing the reaction in air, low conversion (14-17%) was obtained in the presence of **5**, **6**, and **7** (runs 5, 7, and 9) while no reaction was observed for **1**, **8** and **9** (runs 2, 11, and 13). This significant drop of activity was attributed to the hydrolysis of the complexes affording catalytically inactive parental calixarenes; separate runs using the parent calixarenes failed to produce any PCL.

δ-valerolactone (δ-VL)

The ROP of δ-valerolactone (δ-VL) was also investigated. By performing the reaction in toluene and in the presence of BnOH as co-activator, none of the catalysts proved active, affording either nil or trace polymer after 24 h at 130 °C. Furthermore, the tests were repeated under solvent-free conditions (Table 3). Due to the disappointing results achieved in the CL case, the Na-containing species **4** was not further tested. Poor activity was exhibited by complexes **1** and **2**, allowing for 18 and 10% conversion, respectively, after 24 h (runs 1 and 2). Good conversion (58%) was obtained in the presence of the SO_2-bridged derivative **5** after 10 minutes (run 3); however, further reaction was impeded by the formation of a highly viscous mixture. A similar outcome was observed in the presence of complexes **7**-**9**, albeit with longer reaction times (30 min – 12 h, runs 4-6). Finally, complete conversion was attained after 12 h with the dimethyleneoxa-derivative **6**, affording a PVL with M_n lower than the expected values and rather broad polydispersity (1.57, run 4). This indicated the occurrence of extensive transesterification. Noteworthy, the M_w/M_n values observed for the PCLs and PVLs do not present significant differences (with respect to the uncertainty of the GPC measurements). Thus, the same extent of transesterification can be assumed for both monomers. This was primarily attributed to the lack of homogeneity of the reaction medium, as the formation of polymer often impeding efficient stirring of the mixture. On the other hand, M_n higher than the expected values were obtained in the presence of complexes **5** and **7**-**9**, indicating partial catalyst activation. Similar to the ε-CL case, the ^{1}H NMR spectrum of the PVL synthesized with **6** suggested the formation of linear $–CH_2OH$ capped polymer chains (Figure S8). The MALDI-ToF spectrum of the sample highlighted the presence of a main set of peaks (Figure S9) compatible with an α-hydroxyl-ω-(carboxylic acid)-terminated PVL, suggesting that, unlike the PCL case, the polymerization was initiated by adventitious water. Two minor distributions accountable to cyclic species and Na-doped linear adducts were also observed (Figures S10 and S11, respectively).

Table 1. ROP of ε-CL catalysed by the Li complexes.

Run	Catalyst	ε-CL:Li:BnOH	T (°C)	Time (h)	Conversion[a] (%)
1	**1**	100:1:1	130	24	16
2	**2**	100:1:1			0
3	**4**	100:1:1			0
4	**5**	100:1:1			18
5	**6**	100:1:1			10
6	**7**	100:1:1			20
7	**8**	100:1:1			11
8	**9**	100:1:1			7

[a] Determined by ^{1}H NMR spectroscopy on crude reaction mixture.

Table 2. ROP of ε-CL catalysed by the Li complexes under solvent-free conditions.

Run	Catalyst	ε-CL:Li	T (°C)	Time (h)	Conversion[a] (%)	M_n[b,c]	M_{ncalc}[d].	PDI[b]
1	**1**	100:1	130	24	None	-	-	-
2[e]				24	None	-	-	-
3	**2**			24	45	1,800	5,130	1.25
4	**4**			24	None	-	-	-
5	**5**			1[f]	40	14,640	4,560	2.01
6[e]				24	17%	nd		nd
7	**6**			10 min	>99	27,000	11,290	1.67
8[e]				24	17	-	-	-
9	**7**			1[f]	80	16,130	9,130	1.78
10[e]				24	14	-	-	-
11	**8**			15 min[f]	72	27,520	8,210	1.76
12[e]				24	none	-	-	-
13	**9**			6	77	17,040	8,780	2.05
14[e]				24	none	-	-	-

[a] Determined by ^{1}H NMR spectroscopy on crude reaction mixture. [b] From GPC. [c] Values corrected considering Mark–Houwink factor (0.56) from polystyrene standards in THF. [d] Calculated from ([Monomer]$_0$/[Cat.]$_0$) × conv. (%) × Monomer molecular weight. [e] Reaction performed in air. [f] Stirring stopped due to the polymer formation.

rac-Lactide (r-LA)

The complexes were then employed as catalysts in the ROP of *r*-LA under *solvent-free* conditions at 150 °C (Table 4). While low molecular weight oligomers were obtained with **2**, **4**, **5**, **7**, and **9**, wax-like materials were isolated in the presence of the **1**, **6**, and **8**. M_n higher than the calculated values and polydispersities of *ca*. 1.7 suggested partial catalyst activation as well as the occurrence of transesterification. Again, here the dimethyleneoxa-bridged complex **6** performed best. The samples showed high heterotactic enrichment (P_r 0.88-0.91), as observed by 2D *J*-resolved ^{1}H NMR spectroscopy (Figures S12-S14). [26] However, due to the poor activity of the catalysts in solution, it has not been possible to perform mechanistic investigations by NMR spectroscopy in order to assess the type of stereocontrol involved.The MALDI-ToF spectrum of the PLA prepared in the presence of **6** (Figure S15) highlighted the presence of only one population accountable to cyclic species. In addition, the fact that the peaks are separate by 72 m/z units (mono-lactyl group) suggested the occurrence of transesterification.

Table 3. ROP of δ-VL catalysed by the Li complexes under solvent-free conditions.

Run	Catalyst	δ-VL:Li	T (°C)	Time (h)	Conversion[a] (%)	M_n[b,c]	M_{ncalc}[d].	PDI[b]
1	**1**	100:1	130	24	18	nd	1,800	nd
2	**2**			24	10	1,320	1,000	1.29
3	**5**			10 min[f]	58	30,100	5,800	2.12
4	**6**			12	>99	2,990	9,900	1.57
5	**7**			1[f]	46	16,360	4,600	1.29
6	**8**			30 min[f]	60	21,680	6,000	1.52
7	**9**			12[f]	64	31,650	6,400	2.08

[a] Determined by ^{1}H NMR spectroscopy on crude reaction mixture. [b] From GPC. [c] Values corrected considering Mark–Houwink factor (0.56) from polystyrene standards in THF. [d] Calculated from ([Monomer]$_0$/[Cat.]$_0$) × conv. (%) × Monomer molecular weight. [e] Reaction performed in air. [f] Stirring stopped due to the polymer formation.

Table 4. ROP of *r*-LA catalysed by the Li complexes.

Run	Catalyst	*r*-LA:Li	T (°C)	Time (h)	Conversion[a] (%)	M_n[b,c]	M_{ncalc}[d].	PDI[b]	P_r[e]
1	**1**	100:1	150	24	57	17,340	8,210	1.73	0.91
2	**2**	100:1			18		liquid oligomers		
3	**3**	100:1			25	nd	3,600	nd	nd
4	**5**	100:1			69		liquid oligomers		
5	**6**	100:1			87	18,470	12,530	1.72	0.90
6	**7**	100:1			18	nd	1,150	nd	nd
7	**8**	100:1			57	22,650	8,210	1.71	0.88
8	**9**	100:1			66		liquid oligomers		

[a] Determined by ^{1}H NMR spectroscopy on crude reaction mixture. [b] From GPC. [c] Values corrected considering Mark–Houwink factor (0.56) from polystyrene standards in THF. [d] Calculated from ([Monomer]$_0$/[Cat.]$_0$) × conv. (%) × Monomer molecular weight. [e] Determined 2D *J*-resolved ^{1}H NMR spectroscopy.

Table 5. ε-CL/*r*-LA copolymerization catalysed by the Li complexes under solvent-free conditions.

Run	Catalyst	CL:LA:Li	T (°C)	Time (h)	Conversion CL/LA[a] (%)
1	**1**	100:100:1	130	24	0/66
2	**2**				0/80
3	**5**				0/79
4	**6**				0/99
5	**7**				0/70
6	**8**				0/83
7	**9**				0/71

[a] Determined by ^{1}H NMR spectroscopy on crude reaction mixture.

ω-pentadecalactone (ω-PDL)

All complexes were found to be inactive in the ROP of the more challenging 15-membered ring monomer ω-pentadecalactone, both in solution and under *solvent-free* conditions.

ε-CL/r-LA co-polymerization

Lastly, the co-polymerization of ε-CL and *r*-LA was investigated in bulk at 130 °C (Table 5). While ε-CL was completely unreacted, the conversion of *r*-LA was observed, as highlighted by ^{1}H NMR spectroscopy on the crude reaction mixtures (see for example Figure S16). Liquid PLA oligomers, whose separation from the residual monomers proved problematic, were obtained in all cases.

Conclusions

In conclusion, the use of LiO*t*Bu (or LiOH or *n*BuLi in the case of **4** and **7**) on interaction with a series of calixarenes containing a range of bridging groups, namely –CH_2–, –S–, –SO–, –SO_2– or –CH_2OCH_2– allowed access to a number of lithiated calix[3 and 4]arenes (see Chart 1). In the case of the –SO–, adventious oxidation can result in the formation of mixed –SO–/–SO_2– bridging.

All complexes (except **1** and **4**) proved active in the ROP of ε-CL, δ-VL and *r*-LA under *solvent-free* conditions and in the case of CL, the activity trend was found to be **6** > **7** > **8** > **5** > **9**. Similar results were also observed in the case of the other monomers, with the dimethyleneoxa-bridged derivative outperforming the other systems. The higher activity of **6** was thought to be due to the higher flexibility of the −CH_2OCH_2− bridge allowing better access to the active centre(s) and/or to the stabilization of the active species by the oxygen atoms of said bridge. In most of the cases, incomplete catalyst activation and lack of control were observed. The NMR spectroscopy characterization of selected samples suggested the formation of linear –CH_2OH capped PCLs and PVLs and highly heterotactic PLAs. None of the catalysts proved active in the ROP of the larger monomer ω-pentadecalactone, while the conversion of only *r*-LA was observed during ε-CL/*r*-LA co-polymerization.

Conflicts of interest

There are no conflicts to declare

Experimental

General

All manipulations were carried out under an atmosphere of nitrogen using standard Schlenk and cannula techniques or in a conventional nitrogen-filled glove-box. Solvents were refluxed over an appropriate drying agent, and distilled and degassed prior to use. THF-d_8 was stirred over CaH_2 for 48h, vacuum transferred and then stored over 3A molecular sieves. Elemental analyses were performed by the microanalytical services at the London Metropolitan University or the Chemistry Department at the University of Hull. NMR spectra were recorded on a Varian VXR 400 S spectrometer at 400 MHz; chemical shifts are referenced to the residual protio impurity of the deuterated solvent. IR spectra (nujol mulls, KBr windows) were recorded on Perkin-Elmer 577 and 457 grating spectrophotometers. The compounds 1,3-di-*n*-propyloxycalix[4]arene and p-*tert*-butylhexahomotrioxacalix[3]areneH_3 were prepared from using the literature methods. [27] The compound p-*tert*-butylthiacalix[4]areneH_4 was purchased from TCI UK, whilst the ligands p-*tert*-butylsulfinylcalix[4]areneH_4 and p-*tert*-butylsulfonylcalix[4]areneH_4 were gifts from Dr Hitoshi Kumagaya of the Cosmo oil company. The complex [$L^{S4}Li_5$(OH)$(THF)_4$] was prepared by the method of Zeller and Radius. [18] All other chemicals were obtained commercially and used as received unless stated otherwise.

Preparation of [$Li_8(L^{4S})_2(THF)_4$]·5THF (**1**·5THF)

A solution of lithium *tert*-butoxide (7.21 ml, 1M in THF, 7.21 mmol) was added to L^SH_4 (1.00 g, 1.39 mmol) in THF (30 ml) at ambient temperature. After stirring for 1 h, the orange solution was concentrated to about 20 ml, and was left to stand for 48 h at room temperature to afford colourless crystals of **1**·5THF suitable for X Ray diffraction analysis in 65 % yield (0.90 mmol, 1.90 g). Anal. Cald for $C_{56}H_{76}S_8Li_8O_8$: C, 56.58; H, 6.44%; found C, 56.49; H, 6.28 %. IR: 1587w, 1357m, 1306w, 1260s, 1199s, 1093bs, 1022bs, 911w, 885m, 865m, 800bs, 767m, 733m, 702w, 668w, 620w, 546m. MS (M^+): 1488.6 m/z. ^{1}H NMR (THF-d_8, 400 MHz, 298 K) δ: 7.61 (s, 16 H, Ar*H*), 1.31 (s, 72H, (CH_3)$_3$C). ^{7}Li NMR (THF-d_8, 194.3 MHz, 298 K) δ: 1.50 (s).

Preparation of [$Li_6(L^{4SO}H)_2(THF)_2$]·5(THF) (**2**·5THF)

A solution of lithium *tert*-butoxide (2.01 mL, 1M in THF, 2.01 mmol) was added to $L^{SO}H_4$ (0.51 g, 0.65 mmol) in THF (10 ml) at ambient temperature. After stirring for 1h, the solution was

concentrated to about 10 mL, and was left to stand for 48 h at room temperature, to afford colourless crystals of **2**·8THF suitable for X Ray diffraction analysis in 31% yield (0.20 mmol, 0.22 g). Anal. Cald for $C_{88}H_{106}Li_6O_{18}S_8$ (sample dried *in-vacuo* for 12 h, -5THF) requires C 60.40, H 6.11% Found C 59.87, H 6.39%. IR: 2727w, 1772w, 1602m, 1305w, 1093s, 1019s, 878w, 801s, 660w, 643w, 600w, 491w. ^{7}Li NMR (THF-d_8, 194.3 MHz, 298 K) δ: 3.24 (s).

Preparation of $[Li_8(L^{SO/3SO2})_2(THF)_6]$·8(THF) (**3**·8THF)
A solution of lithium *tert*-butoxide (6.62 ml, 1M in THF, 6.62 mmol) was added to $L^{SO}H_4$ (1.00 g, 1.27 mmol) in THF (30 ml) at ambient temperature. After stirring for 1h, the solution was concentrated to about 20 ml, and was left to stand for 48 h at room temperature to afford colourless crystals of **3**·8THF suitable for X Ray diffraction analysis in 70 % yield (0.89 mmol, 2.40 g). Anal. Cald for $C_{136}H_{200}Li_8O_{36}S_8$ requires C 59.98, H 7.40%. Found C 60.19, H 7.39%. IR: 1606w, 1462m, 1377m, 1260m, 1087m, 1020m, 799m, 722w, 566w. ^{1}H NMR (THF-d_8, 400 MHz, 298 K) δ: 7.98-7.70 (m, 16H, Ar*H*), 1.32-1.29 (m, 72H, $(CH_3)_3$C). ^{7}Li NMR (THF-d_8, 194.3 MHz, 298 K) δ: 1.37 (bs).

Preparation of $[Li_5Na(L^{SO/3SO2}H)_2(THF)_5]$·7.5(THF) (**4**·7.5THF)
To $L^{4SO}H_4$ (1.00 g, 1.27 mmol) and LiOH (0.16 g, 6.68 mmol) in THF (30 ml) at ambient temperature. After stirring for 12 h, the system was filtered, concentrated to about 20 ml, and was left to stand for 48 h at room temperature affording colourless prisms of **4**·7.5THF suitable for X Ray diffraction analysis in 26% yield (0.33 mmol, 0.45 g). Anal. Cald for $C_{104}H_{138}Li_5NaO_{28}S_8$ (-7.5THF, sample dried *in-vacuo* for 3h) requires C 58.09, H 6.47%. Found C 58.57, H 6.92%. IR: 3530bs, 2826w, 2360m, 2341w, 1604m, 1261s, 1220w, 1092s, 1020s, 866w, 799s, 723m, 678w, 634w, 563w. ^{1}H NMR (THF-d_8, 400 MHz, 298 K) δ: 8.82 (bs, 2H, -O*H*, 7.97-7.72 (m, 16 H, Ar*H*), 1.25-1.03 (m, 72H, $(CH_3)_3$C). ^{7}Li NMR (THF-d_8, 194.3 MHz, 298 K) δ: 0.14 (bs).

Preparation of $[Li_5L^{4SO2}(OH)(THF)_4]$·2THF (**5**·2THF)
A solution of lithium *tert*-butoxide (6.12 ml, 1M in THF, 6.12 mmol) was added to $L^{SO2}H_4$ (1.00 g, 1.18 mmol) in THF (30 ml) at ambient temperature. After heating at 70 °C for 1h, the solution was filtered hot under nitrogen atmosphere on a POR4 frit, and was left to stand for 48 h at room temperature affording colourless crystals of **5**·2THF suitable for X Ray diffraction analysis in 60 % yield (0.71 mmol, 0.89 g). Anal. Cald for $C_{60}H_{85}S_4Li_5O_{18}$: C, 57.32; H, 6.82%; found C, 57.21; H, 6.85%. IR: 3182bw, 1609m, 1500m, 1396w, 1365m, 1328w, 1292m, 1261s, 1214m, 1197m, 1155m, 1127s, 1080bs, 1019bs, 962m, 902w, 866w, 796s, 735w, 722w, 685w, 660w, 631m, 562m, 523w, 495w, 478w. ^{1}H NMR (THF-d_8, 400 MHz, 298 K) δ: 7.99 (s, 8H, Ar*H*), 1.34 (s, 36H, $(CH_3)_3$C). O*H* signal not detected. ^{7}Li NMR (THF-d_8, 194.3 MHz, 298 K) δ: 1.23 (s).

Preparation of $[Li_6(L^{COC})_2(HOtBu)_2]$·0.78THF·1.22hexane (**6**·0.78THF·1.22hexane)
A solution of lithium *tert*-butoxide (9.02 ml, 1M in THF, 9.02 mmol) was added to $L^{COC}H_4$ (1.00 g, 1.73 mmol) in THF (30 ml) at ambient temperature. After stirring for 1h, the volatiles were removed *in-vacuo*, and the residue was taken up in hexane (30 ml). Filtration of the solution under nitrogen atmosphere on a POR4 frit and cooling at 0 °C afforded colourless crystals of **6**·0.78THF·1.22hexane suitable for X Ray diffraction analysis in 11% yield (0.19 mmol, 0.25 g). Further crops of crystals can be obtained by concentration of the mother liqueur to 10 mL and standing at -40 °C for 10 days (total isolated yield 45%, 0.78 mmol, 1.02 g). $C_{90.45}H_{133.36}Li_6O_{14.77}$ requires C 72.48, H 8.97%. Found C, 71.96; H, 8.49%. IR: 3662 (bs), 2727w, 1636m, 1304w, 1260w, 1260w, 1211m, 1094m,1018m, 975m, 875w, 802m, 722m, 530w. ^{1}H NMR (THF-d_8, 400 MHz, 298 K) δ: 7.08-6.70 (m, 12H, Ar*H*), 5.16-4.81 (m, 12H, *endo*-CH_2), 4.53-4.40 (m, 12H, *exo*-CH_2), 2.27-2.03 (bs, 2H, $(CH_3)_3$CO*H*), 1.30-1.19 (m, 54H,(CH_3)$_3$C)), 1.10 (s, 18H, (CH_3)$_3$COH). ^{7}Li NMR (THF-d_8, 194.3 MHz, 298 K) δ: 0.14 (bs), 0.13 (s).

Preparation of $[LH_2Li_2(thf)(OH_2)_2]$·3THF (**7**·3THF)
A solution of lithium *tert*-butoxide (4.33 ml, 1M in THF, 4.33 mmol) was added to LH_4 (1.00 g, 1.73 mmol) in THF (30 ml) at ambient temperature. After stirring for 4h, the solution was concentrated to about 20 ml, and was left to stand for 48h at room temperature to afford colourless crystals of **7** suitable for X Ray diffraction analysis in 45% yield (0.59 g, 0.78 mmol). $C_{60}H_{90}Li_2O_{10}$ requires C 73.14, H 9.21%. Found C, 71.48; H, 10.35%. [28] IR: 3611s, 3476w, 2727w, 2360w, 1744w, 1603w, 1577w, 1303s, 1155w, 1130m, 1104w, 1040s, 967w, 910m, 871s, 821m, 795m, 736s, 668w, 606m. ^{1}H NMR (THF-d_8, 400 MHz, 298 K) δ: 7.13-6.76 (m, 16H, Ar*H*), 5.08 (d, 2H, *J* = 12 Hz, *endo*-CH_2), 4.66 (d, 2H, *J* = 12 Hz, *endo*-CH_2), 4.57 (d, 2H, *J* = 12 Hz, *endo*-CH_2), 4.14 (d, 2H, *J* = 12 Hz, *endo*-CH_2), 3.40-3.02 (m, 8H, *exo*-CH_2), 1.43-1.11 (m, 72H, (CH_3)$_3$C). O*H* signal not detected. ^{7}Li NMR (THF-d_8, 194.3 MHz, 298 K) δ: 2.44 (bs), 1.77 (bs).

Preparation of $\{[Li_5(de\text{-}BuL)(OH)(NCMe)_3]$·2MeCN$\}_n$ (**8**·2MeCN)
A solution of lithium *tert*-butoxide (12.25 ml, 1M in THF, 12.25 mmol) was added to de-BuLH_4 (1.00 g, 2.36 mmol) in THF (30 ml) at ambient temperature. After stirring for 4h the volatiles were removed *in-vacuo*, and the residue was taken up in MeCN (30 ml). Filtration under nitrogen atmosphere on a POR4 frit and cooling at 0 °C afforded, after 1 day, colourless crystals of **8**·2MeCN suitable for X Ray diffraction analysis in 55 % yield (1.30 mmol, 0.88 g). Cald. for $C_{38}H_{36}Li_5N_5O_5$ (-MeCN, sample dried *in-vacuo* for 2h) C 67.94, H 5.23, N 8.81%. Found C 69.31, H 5.77, N 8.84%. [28] Found C 65.76, H 5.86, N 2.04%. IR: 3609w, 1587w, 1301m, 1288m, 1261s, 1218w, 1092bs, 1046s, 1020bs, 944w, 909w, 860w, 847m, 800s, 752m, 723w, 705w, 678w. ^{1}H NMR (THF-d_8, 400 MHz, 298 K) δ: 7.85-7.76 (m, 8H, Ar*H*), 7.04-6.64 (m, 8H, Ar*H*), 6.24-5.99 (m, 8H, Ar*H*), 5.10 (d, 2H, *J* = 13 Hz, *endo*-CH_2), 4.94 (d, 2H, *J* = 13 Hz, *endo*-CH_2), 4.64 (d, 2H, *J* = 13 Hz, *endo*-CH_2), 4.17 (d, 2H, *J* = 13 Hz, *endo*-CH_2), 3.61 (d, 2H, J = 12 Hz, *exo*-CH_2), 3.41-3.03 (m, 6H, *exo*-CH_2), 2.08 (s, 12H, MeCN), 1.29 (s, 6H, MeCN).^{7}Li NMR (THF-d_8, 194.3 MHz, 298 K) δ: 3.46 (s), 0.46 (bs), -2.36 (bs).

Preparation of $[Li_6(L^{Pr})_2(H_2O)_2]$·hexane (**9**·hexane)

To a solution of $L^{Pr^2}H_2$ (1.00 g, 1.36 mmol) in THF (30 ml) at – 78 °C was added *n*BuLi (4.35 ml, 1.6 M, 2.75 mmol). After stirring for 12 h at ambient temperature, the volatiles were removed *in-vacuo*, and the residue was taken up in hexane (30 ml). Filtration of the solution under nitrogen atmosphere on a POR4 frit and cooling to 0 °C afforded, after 3 days, small colourless crystals of **9**·hexane suitable for X Ray diffraction analysis in 25 % yield (0.34 mmol, 0.52 g). Anal. Cald for $C_{100}H_{136}Li_6O_{10}$: C, 78.00; H, 8.90%; found C, 77.67; H, 8.78%. IR: 3376bm, 3182w, 1747w, 1671w, 1598s, 1337m, 1301s, 1261s, 1236m, 1194s, 1096s, 1055bs, 969s, 917w, 871s, 799s, 755w, 723m, 675w, 633w. ^{1}H NMR (THF-d_8, 400 MHz, 298 K) δ: 7.03-6.95 (m, 8H, Ar*H*), 6.90-6.45 (m, 8H, Ar*H*), 6.60-6.33 (m, 8H, Ar*H*), 4.31 (d, 4H, *J* = 12 Hz, *endo*-CH_2), 4.12 (d, 4H, *J* = 13 Hz, *endo*-CH_2), 3.92 (t, 4H, J = 7 Hz, -OCH_2CH$_2$CH$_3$), 3.30 (d, 4H, J = 13 Hz, *exo*-CH$_2$), 3.95 (d, 4H, J = 12 Hz, *exo*-CH_2), 2.06 (m, 4H, -OCH$_2$CH_2CH$_3$), 1.32 (t, 6H, -OCH$_2$CH$_2$CH_3). ^{7}Li NMR (THF-d_8, 194.3 MHz, 298 K) δ: 2.17 (s), 1.55 (bs).

Ring open polymerization (ROP) procedures

Reaction in toluene: Under inert atmosphere, a THF solution of the complex (1 mM) was added into a Schlenk tube and the solvent was removed under reduced pressure at room temperature. Toluene (2 mL) was added along with the monomer (4.5 mmol) and the required amount of BnOH (as a toluene solution). The reaction mixture was then placed into an oil bath pre-heated to the required temperature, and the solution was stirred for the prescribed time. The polymerization mixture was then quenched by addition of an excess of glacial acetic acid (0.2 mL) into the solution, and the resultant solution was then poured into methanol (200 mL). The resultant polymer was then collected on filter paper and dried in air at room temperature.

Solvent-free conditions: Under an inert atmosphere, a THF solution of the complex (1 mM) was added into a Schlenk tube and the solvent was removed under reduced pressure at room temperature. The monomer (9.0 mmol) was then added and the reaction was stirred at 130 °C for 12-24 h, or until a mass of polymer blocking the stirring formed. The mixture was then taken up in CH_2Cl_2 and quenched with acidified methanol (200 mL). The resultant polymer was then collected on filter paper and dried in air at room temperature.

Crystal Structure Determinations

Diffraction data for **1**·5THF, **5**·2THF, & **8**·2MeCN were collected on a Bruker Apex 2 CCD diffractometer using a sealed tube source; for **2**·5THF & **7**·3THF at the Diamond Light Source synchrotron, station I19, equipped with Rigaku Saturn724+ CCD or Crystal Logic diffractometers; for **3**·8THF, **4**·7.5THF, and **6**·0.78THF·1.22hexane, on Rigaku Saturn 724+ CCD diffractometers equipped with sealed tube (**3**·8THF & **4**·7.5THF) or rotating anode (**6**·0.78THF·1.22hexane) sources; and for **9**·hexane at the Advanced Light Source synchrotron, Station 11.3.1, equipped with a Bruker Apex 2 CCD diffractometer. Further details are given in Table 5 and in the deposited cif files. All crystal structures were collected at low temperature. Data were corrected for absorption and Lp effects. The structures were solved using direct methods [29] or a dual-space, charge-flipping algorithm and refined on F^2. [30, 31] This set of lithium-containing calixarene structures were challenging due to often weak diffracting power caused by their light-atom make-up, and the often-encountered *t*Bu group and solvent of crystallization disorder. Some *t*Bu groups needed to be modelled with the methyl groups or the whole moiety split over two sets of positions. Solvent molecules of crystallization were often disordered and needed to be modelled with split positions, or as diffuse electron density via the Platon Squeeze procedure (for **1**·5THF, **2**·5THF, **4**·7.5THF, and **5**·2THF). [32] The 'squeezed' solvent contribution is included in the chemical formula in each case. The number of solvent molecules of crystallization should only be taken as approximate. Where disorder has been modelled, restraints were applied to anisotropic displacement parameters and the geometry of the affected and immediately adjacent atoms. For **2**·5THF there was some evidence of partial disorder in the O atom on each –SO– bridging group, with the O sometimes positioned in the other tetrahedral site on the S; this was modelled and the major components at O(5), O(6), O(7), and O(8) were 88.4(8), 91.4(7), 81.6(8), and 81.9(9)%, respectively. For **3**·8THF the occupancies of O(6) and O(11) were refined as 68.1(10) and 68.0(10%, respectively. For **4**·7.5THF O(20) was only 78.0(18)% occupied. For **5**·2THF both THFs are disordered along the 4-fold axis and both were modelled with 'Squeeze'. One resides in the calixarene cavity, the other above the coordinated THFs. In **6**·0.78THF·1.22hexane the solvent of crystallization site was provisionally modelled with point atoms as having part hexane and part THF in a 61.2:38.8(4) % ratio, but due to the severity of the disorder was subsequently modelled with the Platon Squeeze procedure.[32] Atoms O(7)/H(7) were modelled a two-fold disordered with major site occupancy of 54.9(12)% while atoms O(6)/C(36) and the associated hydrogens were also modelled as two-fold disordered with major site occupancy 85.2(4)%. The diffraction data for **8**·2MeCN were non-merohedrally twinned via a 180° rotation about real axis 0 0 1 with a twin component ratio of 52.2:47.8(4) %. Hydrogen atoms were placed in geometrically determined positions, except for those on hetero atoms in structures with good data, where coordinates were refined.

CCDC 2038615-23 contain the crystal data for the structures reported herein.

Table 5. Crystallographic data for complexes **1** – **9**

Compound	**1**·5THF	**2**·5THF	**3**·8THF	**4**·7.5THF	**5**·2THF
Formula	$C_{116}H_{160}S_8Li_8O_{17}$	$C_{108}H_{146}Li_6O_{23}S_8$	$C_{136}H_{200}Li_8O_{34.72}S_8$	$C_{134}H_{198}Li_5NaO_{35.28}S_8$	$C_{60}H_{85}S_4Li_5O_{18}$
Formula weight	2138.43	2110.36	2702.48	2687.55	1257.21
Crystal system	Monoclinic	Triclinic	Monoclinic	Monoclinic	Tetragonal
Space group	*I*2/*a*	*P*$\bar{1}$	$P2_1/c$	*C*2	*P*4/*n*
Unit cell dimensions					
a (Å)	25.323(13)	13.354(12)	17.8795(13)	38.167(3)	13.306(2)
b (Å)	17.655(9)	13.959(9)	23.8479(17)	20.3517(14)	13.306(2)
c (Å)	26.894(14)	17.735(14)	17.9950(13)	18.4867(13)	19.079(3)
α (º)	90	70.39(4)	90	90	90
β (º)	105.218(5)	84.17(5)	111.9050(11)	99.9979(5)	90
γ (º)	90	62.02(3)	90	90	90
V (Å^3)	11602(10)	2744(4)	7118.9(9)	14141.7(18)	3377.9(9)
Z	4	1	2	4	2
Temperature (K)	150(2)	100(2)	100(2)	100(2)	150(2)
Wavelength (Å)	0.71073	0.6889	0.71073	0.71073	0.71073
Calculated density (g.cm^{-3})	1.224	1.277	1.261	1.262	1.236
Absorption coefficient (mm^{-1})	0.216	0.231	0.199	0.203	0.205
Transmission factors (min./max.)	0.950 and 0.981	0.984 and 0.998	0.965 and 0.982	0.672 and 1.000	0.941 and 0.984
Crystal size (mm^3)	0.24 × 0.11 × 0.09	0.07 × 0.05 × 0.01	0.18 × 0.17 × 0.09	0.25 × 0.20 × 0.12	0.30 × 0.22 × 0.08
ϑ(max) (°)	22.5	26.6	27.6	27.5	25.0
Reflections measured	35870	27343	66538	98566	26220
Unique reflections	7584	12071	16117	32341	2987
R_{int}	0.230	0.183	0.110	0.047	0.081
Reflections with $F^2 > 2\sigma(F^2)$	2884	3704	13043	30584	2071
Number of parameters	748	707	965	1657	191
R_1 [$F^2 > 2\sigma(F^2)$]	0.098	0.109	0.0973	0.063	0.064
wR_2 (all data)	0.272	0.329	0.280	0.176	0.187
GOOF, *S*	0.93	0.88	1.07	1.05	1.08

Largest difference peak and hole (e $Å^{-3}$)	0.41 and –0.32	0.53 and –0.31	1.08 and –0.88	1.17 and –0.40	0.67 and –0.43

Compound	**6**·0.78THF·1.22hexane	**7**·3THF	**8**·2MeCN	**9**·hexane
Formula	$C_{90.45}H_{133.36}Li_6O_{14.77}$	$C_{60}H_{90}Li_2O_{10}$	$C_{38}H_{36}Li_5N_5O_5$	$C_{100}H_{136}Li_6O_{10}$
Formula weight	1498.68	985.19	677.42	1539.3
Crystal system	Triclinic	Monoclinic	Monoclinic	Triclinic
Space group	$P\bar{1}$	$P2_1$	$P2_1/m$	$P\bar{1}$
Unit cell dimensions				
a (Å)	13.350(8)	11.763(14)	13.011(7)	10.5688(9)
b (Å)	13.868(9)	36.82(4)	10.480(6)	13.1163(11)
c (Å)	14.564(9)	13.119(16)	13.837(8)	17.2651(14)
α (º)	114.022(7)	90	90	102.6019(11)
β (º)	95.245(6)	96.406(11)	112.332(8)	91.2345(12)
γ (º)	111.486(6)	90	90	93.5123(12)
V (Å^3)	2198(2)	5647(11)	1745.2(17)	2329.8(3)
Z	1	4	2	1
Temperature (K)	100(2)	100(2)	150(2)	150(2)
Wavelength (Å)	0.71073	0.6889	0.71073	0.7749
Calculated density (g.cm^{-3})	1.132	1.159	1.289	1.097
Absorption coefficient (mm^{-1})	0.074	0.075	0.084	0.080
Transmission factors (min./max.)	0.980 and 0.993	0.340 and 1.000	0.974 and 0.997	0.990 and 0.993
Crystal size (mm^3)	0.28 × 0.16 × 0.09	0.06 × 0.05 × 0.02	0.31 × 0.24 × 0.04	0.15 × 0.10 × 0.10
ϑ(max) (°)	31.5	22.5	26.5	33.6
Reflections measured	29498	37790	20601	34077
Unique reflections	12781	15742	6965	13962
R_{int}	0.039	0.133	0.199	0.061
Reflections with $F^2 > 2\sigma(F^2)$	8911	9255	2595	9552
Number of parameters	493	1333	298	561
R_1 [$F^2 > 2\sigma(F^2)$]	0.071	0.150	0.115	0.072
wR_2 (all data)	0.215	0.451	0.276	0.228
GOOF, S	1.05	1.05	1.04	1.06

Largest difference peak and hole (e Å^{-3})	0.44 and –0.36	0.56 and –0.49	0.40 and –0.52	0.66 and –0.36

Acknowledgements

We thank the EPSRC for funding (EP/R023816/1 and EP/S025537/1), and the EPSRC National Crystallography Service at Southampton (UK) and the EPSRC Mass Spectrometry Service, Swansea (UK) for data collection. This research used resources of the Advanced Light Source, which is a DOE Office of Science User Facility under contract no. DE-AC02-05CH11231.

Notes and references

1 (a) R. E. Drumright, P. R. Gruber and D. E. Henton, *Adv. Mater*. 2000, **12**, 1841−1846; (b) C. K. Williams and M. A. Hillmyer, *Polym. Rev.* 2008, **48**, 1−10; (c) M. A. Woodruff and D. W. Hutmacher, *Prog. Polym. Sci.* 2010, **35**, 1217−1256; (d) A. L. Sisson, D. Ekinci and A. Lendlein, *Polymer* 2013, **54**, 4333−4350.

2 (a) A. Arbaoui and C. Redshaw, *Polym. Chem.* 2010, **1**, 801–826; (b) I. Nifant'ev and P. Ivchenko, *Molecules* 2019, **24**, 4117; (c) O. Santoro, X. Zhang and C. Redshaw, *Catalysts* 2020, **10**, 800.

3 D. Homden and C. Redshaw, *Chem. Rev*. 2008, **108**, 5086-5130.

4 O. Santoro and C. Redshaw, *Catalysts* 2020, **10**, 210.

5 C. Floriani and R. Floriani-Moro, *Adv. Organomet. Chem*. 2001, **47**, 167-233.

6 See for example (a) B. Masci in *Calixarenes 2001*, Eds. Z. Asfari, V. Böhmer, J. Harrowfield and J. Vicens, Kluwer Academic Publishers 2001, Chapter 12; (b) N. Morohashi, F. Narumi, N. Iki, T. Hattori and S, Miyano, *Chem. Rev*. 2006, **106**, 5291-5316; (c) K. Cottet, P. M. Marcos and P. J. Cragg, *Beilstein J. Org. Chem*. 2012, **8**, 201–226.

7 (a) A. K. Sutar, T. Maharana, S. Dutta, C. -T. Chen and C. Lin, *Chem. Soc. Rev*. 2010, **39**, 1724-1746; (b) J. Gao, D. Zhu, W. Zhang, G. A. Solan, Y. Ma and W. -H. Sun, *Inorg. Chem. Front*. 2019, **6**, 2619-2652.

8 (a) C. D. Gutsche, M. Iqbal, K. S. Nam, K. See and I. Alam, *Pure Appl. Chem*. 1988, **60**, 483-488; (b) R. Abidi, M. V. Baker, J. M. Harrowfield, D. S.-C. Ho, W. R. Richmond, B. W. Skelton, A. H. White, A. Varnek and G. Wipff, *Inorg. Chim. Acta* 1996, **246**, 275-286; (c) K. C. Nam, D. S. Kim and J. M. Kim, *Bull. Korean Chem. Soc.* 1997, **18**, 636-640; (d) For FTIR studies see B. Brzezinski, F. Bartl and G. Zundel, *J. Phys. Chem. B*. 1997, **101**, 5611-5653.

9 H. Bock, A. John, C. Nather and Z. Havlas, *J. Am. Chem. Soc*. 1995, **117**, 9367-9368.

10 M. G. Davidson, J. A. K. Howard, S. Lamb, C. W. Lehmann *Chem. Commun*. 1997, 1607-1608.

11 G. Guillemot, E. Solari, C. Rizzoli and C. Floriani, *Chem. Eur. J*. 2002, **8**, 2072-2080.

12 E. D. Gueneau, K. M. Fromm, H. Goesmann, *Chem. Eur. J*. 2003, **9**, 509-514.

13 T. A. Hanna, L. Liu, A. M. Angeles-Boza, X. Kou, C. D. Gutsche, K. Ejsmont, W. H. Watson, L. N. Zakharov, C. D. Incarvito and A. L. Rheingold, *J. Am. Chem. Soc*. 2003, **125**, 6228-6238.

14 D. Mendoza-Espinosa, B. A. Martinez-Ortega, M. Quiroz-Guzman, J. A. Golen, A. L. Rheingold and T. A. Hanna, *J. Organomet. Chem*. 2009, **694**, 1509-1523.

15 L. Liu, L. N. Zakharov, J. A. Golen, A. L. Rheingold, W. H. Watson and T. A. Hanna, *Inorg. Chem*. 2006, **45**, 4247-4260.

16 N. P. Clague, J. D. Crane, D. J. Moreton, E. Sinn, S. J. Teat, N. A. Young, *J. Chem. Soc., Dalton Trans*., 1999, 3535-3536.

17 D. S. Lee, M. R. J. Elsegood, C. Redshaw and S. Zhan, *Acta Cryst*. 2009, **C65**, m291-m295.

18 J. Zeller and U. Radius, *Inorg. Chem*. 2006, **45**, 9487-9492.

19 C. Redshaw, O. Rowe, D. L. Hughes, A. M. Fuller, I. Alvarado Ibarra and S. M. Humphrey, *Dalton Trans*. 2013, **42**, 1983 - 1986.

20 M. Yamada, M. R. Gandhi and F. Hamada, *Acta Cryst. E. Cryst. Comm*. 2018, **74**, 575-579.

21 (a) B. –T. Ko and C. –C. Lin, *J. Am. Chem. Soc*. 2001, **123**, 7973-7977; (b) M. H. Chisholm, C. –C. Lin, J. C. Gallucci and B. –T. Ko, *Dalton Trans*. 2003, 406-412; (c) C. –A. Huang and C. –T. Chen, *Dalton Trans*. 2007, 5561-5566; (d) W. Clegg, M.G. Davidson, D.V. Graham, G. Griffen, M.D. Jones, A.R. Kennedy, C.T. O'Hara, L. Russo and C.M. Thomson, *Dalton Trans*. 2008, 1295-1301; (e) Y. Huang, Y. –H. Tsai, W. –C. Hung, C. –S. Lin, W. Wang, J. –H. Huang, S. Dutta and C. –C. Lin, *Inorg. Chem*. 2010, **49**, 9416-9435; (f) W. –Y. Lu, M. –W. Hsiao, S. C. N. Hsu, W. –T. Peng, Y. –J. Chang, Y. –C. Tsou, T. –Y. Wu, Y. –C. Lai, Y. Chen and H. –Y. Chen, *Dalton Trans*. 2012, **41**, 3659-3667; (g) N. Ikpo, C. Hoffmann, L.N. Dawe and F. M. Kerton, *Dalton Trans*. 2012, **41**, 6651-6660; (h) R. K. Dean, A. M. Reckling, H. Chen, L.N. Dawe, C.M. Schneider and C. M. Kozak, *Dalton Trans*. 2013, **42**, 3504-3520; (i) J. Char, O. G. Kulyk, E. Brulé, F. de Montigny, V. Guérineau, T. Roisnel, M. J. -L. Tschan and C. M. Thomas, Comptes Rendus Chimie, 2016, **19**, 167-172; (j) D. Alhashmialameer, N. Ikpo, J. Collins, L.N. Dawe, K. Hattenhauer and F. M. Kerton, *Dalton Trans*. 2015, **44**, 20216-20231; (k) Y. F. Al-Khafaji, T. J. Prior, L. Horsburgh, M. R. J. Elsegood and C. Redshaw, *Chem*. *Select* 2017, **2**, 759-768.

22 C. Redshaw, *Dalton Trans*. 2016, **45**, 9018 – 9030.

23 (a) P. v. d. Sluis and A. L. Spek, *Acta Cryst*., 1990, **A46**, 194. (b) A. L. Spek, *Acta Cryst*., 2015, **C71**, 9.

24 O. Santoro, M. R. J. Elsegood, E. V. Bedwell, J. A. Pryce and C. Redshaw, *Dalton Trans*. 2020, **49**, 11978-11996.

25 C. Redshaw, M. A. Rowan, L. Warford, D. M. Homden, A. Arbaoui, M. R. J. Elsegood, S. H. Dale, T. Yamato, C. Pérez-Casas, S. Matsui and S. Matsuura, *Chem. Eur. J.* 2007, **13**, 1090.

26 (a) C. Ludwig and M. R. Viant, *Phytochem. Anal*. 2010, **21**, 22; (b) M. J. Walton, S. J. Lancaster and C. Redshaw, *ChemCatChem* 2014, **6**, 1892.

27 (a) A. Arduini, A. Casnati in *Macrocycle Synthesis* (Ed.: D. Parker), Oxford University Press, New York, 1996, chapter 7; b) P. D. Hampton, Z. Bencze, W. Tomg and C. E. Daitch, *J. Org. Chem*. 1994, **59**, 4838-4843.

28 Problems with obtaining satisfactory elemental analysis due to rapid decomposition of compounds of this type were noted by Fromm *et. al*., see reference 12.

29 Sheldrick, G.M., *Acta Cryst*. 2008, **A64**, 112-122.

30 G.M. Sheldrick, *Acta Cryst*. 2015, **A71,** 3-8.

31 G.M. Sheldrick, *Acta Cryst*. 2015, **C71,** 3-8.

32 (a) Spek, A. L. Acta Cryst. 2015, **C71**, 9-18. (b) P.v.d. Sluis and A.L. Spek, *Acta Cryst*. 1990, **A46**, 194-201.